Article

Distributed MPC Method for Power Systems Frequency Control: A Particle Filter Integrated Model for Uncertainty Quantification

Gian Paramo [1] and Arturo Bretas [1,2]

[1] University of Florida, Gainesville, FL 32608
[2] Pacific Northwest National Laboratory, Richland, WA 99352
* Correspondence: arturo.bretas@pnnl.gov

Abstract: The reactive nature of traditional frequency stability methods can lead to delayed corrective actions and unnecessary loss-of-load. This work presents a distributed model predictive control method for proactive power system frequency stability. Dynamic state estimation model is derived through a particle filter. By being able to estimate the future state of frequency, corrective actions can be taken before the system reaches a critical condition. Proactive approach makes it possible to optimize the response to a disturbance, which results in a decrease of the amount of compensation utilized. The method is tested via Matlab simulations based on Kundur's Two-Area System, and the IEEE 14-Bus system. Performance metrics are provided and evaluated against other contemporary solutions found in literature. Easy-to-derive model, without hard-to-design parameters, indicate potential towards real-life applications.

Keywords: Frequency Control, Model Predictive Control, Particle Filter, Phasor Measurement Units, Power Systems.

1. Introduction and Motivation

Traditional frequency stability methods are inherently reactive, and do not have the ability to adapt to the dynamic behavior of the modern grid. Islands and frequency thresholds are currently identified via simulations [1]. This means that contingency plans are created for only a finite number of scenarios [2]. This leads to undesirable results including delayed response, overshedding, and uncoordinated response [3]. In this work, the term *traditional frequency stability methods*, refers to those requiring human interaction, and those based on fixed thresholds derived from simulations. Given their reactive nature, these methods take corrective actions once the system is in a critical state [4].

Many formal mathematical modeling [7] and integrated machine learning methods have otherwise been proposed for prediction. Integrated variational modal decomposition(VMD), particle filter (PF) and Gaussian process regression (GPR) [8], integrated long short-term memory neural network (LSTM NN) and broad learning systems (BLS) [9], and integrated particle swarm optimization (PSO) and BLS [10] are some included in the relevant literature.

Leveraging on the core idea of prediction through integrated models, this work presents a proactive distributed model predictive control (MPC) method for power systems frequency stability. The method considers Phasor Measurement Units (PMUs) observations and the particle filter (PF) for uncertainty quantification. This solution eliminates the need for simulations, utilizes adaptive parameters, and is able to optimize corrective actions.

The concept and its steps are summarized as follows:

1. Disturbances are detected using the rate of change of frequency (RoCoF).
2. The state of frequency is predicted one to three seconds into the future.
3. A load excess factor is determined using the predicted state of frequency.

 doi:10.20944/preprints202304.0599.v1

4. Using loading data collected at the feeder level, the method finds a suitable combination of load (feeders) that will be dropped in stages to meet the excess load factor and regain load-generation balance.

Further, state estimation model is adapted based on PMU observations and a frequency target of 60 Hz is used for reference. Future states are controlled by either actuating Distributed Energy Resources (DERs) or shedding load. These control actions are optimized and executed iteratively.

The rest of this paper is organized as follows: Section 2 provides a brief overview of related techniques found in literature. Theoretical background is presented in Section 3. An overview of the proposed solution along with an illustrative example are given in Section 4. Comparative case studies are found in Section 5. Finally, concluding remarks are given in Section 6.

2. State-of-the-Art

A solution that predicts the final state of frequency after a disturbance is presented in [5]. This method derives an approximate model from PMU readings, and when a disturbance is detected it predicts a new steady state operating point. With the predicted value at hand, the amount of load to be shed which will bring the system back to normal operating conditions is calculated. Some of the highlights of this technique are that very few assumptions are made in the context of inertia and generator governors. However, the performance of [5] is highly dependent on the system being observable, and the time needed for the predicted frequency to converge will vary. In some cases it can take up to two seconds for the algorithm to provide a load excess factor. This uncertainty in regards to processing time is a important limitation. For this reason this solution is suited for systems with high inertia where processing time requirements are not as stringent.

In [6] curves are projected a few seconds into the future to estimate the future state of frequency. Polynomial curve fitting is used to produce these predictions. One of the main appeals of this technique is its simplicity, however, perhaps to due to this such, the technique has several limitations. First, high PMU sampling rates are used. This is a critical parameter that determines the feasibility of the technique, as higher sampling rates place a significant burden on communication systems [11]. Second, in [6] the algorithm alternates between first and second degree polynomials based on assumptions and without feedback. Finally, the authors assume that deviations will follow a mostly linear pattern. These limitations put a constraint on the type of systems where this technique can be implemented.

Power measurements and power injections have also been proposed as a means of monitoring and controlling power system stability. In [12] DERs are actuated to compensate generation-load imbalances. The method uses the Extended Kalman filter to drive DERs in real-time. A frequency stability solution based on monitoring the active power injections of Synchronous Condensers (SCs) is presented in [13]. A novel aspect of this method is that it offers an alternative to RoCoF detection. The premise of this method is that valuable information such as the loss of a generating unit can be retrieved from the change in the active power injection of an SC. It is suggested that disturbances that can be detected earlier by monitoring power injections of SCs compared to RoCoF based methods. In [14], a predictive transient stability monitoring method was presented. After a disturbance occurs, the center of oscillations (CoO) triggered by the disturbance is located. This is achieved by relating the frequencies at two ends of a line. Once the location of the CoO has been identified, a simplified equivalent model of the generator affected by the disturbance is created. By monitoring the potential energy of the system simultaneously with the total energy (the sum of potential and kinetic energies), the generator can be seen drifting into instability before any thresholds are surpassed.

The method developed in this work aims to deliver a performance comparable to that of [5], [6], and [12] while making the following contributions to the state-of-the-art:

- The development of a distributed MPC method for frequency control.

Preprints (www.preprints.org) | NOT PEER-REVIEWED | Posted: 20 April 2023 doi:10.20944/preprints202304.0599.v1

- The use of adaptive thresholds and feedback.
- Optimizing corrective actions via simple optimization routines.
- Addressing concerns related to PMU sampling rates, communication delays, and processing times.

3. Theoretical Background

3.1. Particle Filter

In recent years Bayesian estimators have gained momentum in applications related to power systems. A prominent Bayesian estimator, the Kalman filter (KF), has provided encouraging results, particularly in the area of state estimation [15]. Despite the positive results, some limitations of the KF are becoming evident. Chief among them is the assumption that data processed by the filter always follows a Gaussian distribution. It has been suggested that this assumption is often inadequate as data can follow a variety of probability distributions [16]. A different type of filter, the particle filter (PF), offers a solution to this problem by estimating probability distributions via particles. The PF complements those statistical models with data produced by an underlying system model [17]. At each time step, predictions and corrections are made similar to the Kalman filtering process. An overview of the probability estimation process conducted by the PF is shown in Figure 1.

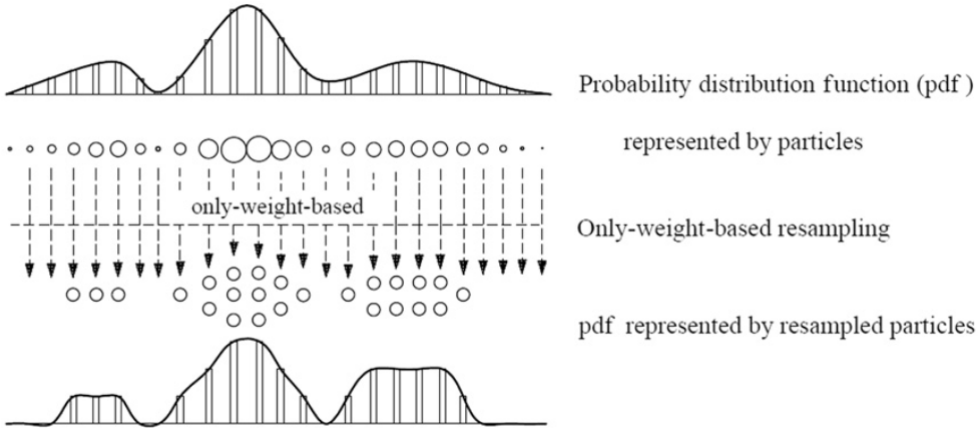

Figure 1. PDF Estimation via Particles [18].

In terms of mathematical formal models, the PF combines elements from the Monte Carlo method and Bayesian estimation. The estimated state along with uncertainties is calculated from probability density functions (PDFs) as described in equation 1 [19]:

$$p(x_k|u_{1:k}, z_{1:k}) \tag{1}$$

Here p is the posterior obtained from a PDF with inputs $u_{1:k}$, and measurements $z_{1:k}$. Each time step produces a new estimate p. Taking the sequence of probabilities produced by 1 and modeling it as a Markov chain, leads to an interesting and useful result in 2:

$$p(x_k|x_{1:k-1}, z_{1:k-1}) = p(x_k|x_{k-1}),\ p(z_k|x_{1:k}) = p(z_k|x_k) \tag{2}$$

Equation 2 suggests that the trajectory of the state from time step $k-1$ to k, can be obtained with reasonable accuracy by simply processing inputs, measurements, and probabilities obtained during the previous time step. The process so far can be summarized using Bayes' theorem:

$$posterior = \frac{likelihood \cdot prior}{marginallikelihood} \tag{3}$$

Preprints (www.preprints.org) | NOT PEER-REVIEWED | Posted: 20 April 2023 doi:10.20944/preprints202304.0599.v1

In equation 3, the *likelihood* comes from a statistical model, while the *prior* comes from a process model. In the denominator, *marginallikelihood*, is used to normalize the *posterior* depending on the nature of the measurements.

The process model mentioned above provides an estimate of how states evolve over time. It can also include noise and other uncertainties. This can be defined as:

$$x_k = f_k(x_{x-1}, u_k, v_{k-1}) \tag{4}$$

Where f combines noise v_{k-1}, inputs u_k, and the previous state x_{x-1} to provide an updated state x, at time step k.

Being a Bayesian filter, the PF updates its prior and posterior at each time step. Given a process model, the prior can be updated using the following equation:

$$p(x_k|z_{1:k-1}) = \int p(x_k|x_{k-1})p(x_{k-1}|z_{1:k-1})dx_{x-1} \tag{5}$$

This prior is a guess based on information received up to time step $k-1$. With this prior, Bayes' theorem can be utilized to obtain the new posterior as:

$$p(x_k|z_{1:k}) = \frac{p(z_k|x_k)p(x_k|z_{1:k-1})}{p(z_k|z_{1:k-1})} \tag{6}$$

Similarly, at each time step, the normalizing constant is updated per 7 below:

$$p(z_k|z_{1:k-1}) = \int p(z_k|x_k)p(x_k|z_{1:k-1})dx_x \tag{7}$$

The steps described so far are very similar to the steps involved in Kalman filtering. A key feature that differentiates the PF from the KF, is the PF's use of the Monte Carlo method. When searching for an optimal Bayesian solution, the PF evaluates a sum of weighted samples, known as particles:

$$p(x_{0:k}|z_{1:k}) \approx \Sigma_{i=1}^{N_s} w_k^i \delta(x_{0:k} - x_{0:k}^i) \tag{8}$$

In equation 8, N_s represents the number of samples in a set. $\delta(\cdot)$ refers to the Dirac delta function. w_k^i represents the weight of each particle $x_{0:k}^i$. w_k^i is computed as:

$$w_k^i \; \alpha \; w_{k-1}^i \frac{p(z_z|x_k^i)p(x_k^i|x_{k-1}^i)}{q(x^i|x_{k-1}^i, z_k)} \tag{9}$$

Subsequent mathematical manipulations of equations 8 and 9, yield equation 10:

$$p(x_k|z_{1:k}) \approx \Sigma_{i=1}^{N_s} w_k^i \delta(x_k - x_k^i) \tag{10}$$

An important principle of the PF can be observed through 10, which is that the solution approaches the real values as the number of particles is increased [19].

Another pivotal element of the PF process is the concept of resampling. Resampling in the PF is analogous to the correction step in the KF. The PF resamples with the goal of correcting imbalances in particle weights [17]. A pseudo-code of the particle filtering process is presented in the following:

Preprints (www.preprints.org) | NOT PEER-REVIEWED | Posted: 20 April 2023 doi:10.20944/preprints202304.0599.v1

Algorithm 1 Particle filter with resampling

Input $\{x_{k-1}^i, w_{k-1}^i\}_{i=1}^{N_s}, z_k$
Output $\{x_k^i, w_k^i\}_{i=1}^{N_s}$
$w_{sum=0}$
for $i = 1, ..., N_s$ **do**
  draw sample $x_k^i \approx q(x_k^i | x_{k-1}^i, z_k)$
  assign weight w_k^i using (2)
  $w_{sum} = w_{sum} + w_k^i$
end for
for $i = 1, ..., N_s$ **do**
  $w_k^i = w^i / w_{sum}$
end for
Resample N_s particles with replacement
for $i = 1, ..., N_s$ **do**
  $w_k^i = 1/N_s$
end for

The system model used in this work is a simple sinusoidal. This underlying model was chosen because it is consistent with the oscillatory behavior of power system frequency.

In conclusion, the PF can be considered an extension of the KF. An extension capable of processing probabilities derived from multiple probability distributions (in Monte Carlo fashion), while adjusting its parameters at each time step, as it is done in Kalman filtering. Overall the trade-off for this increase in flexibility is a modest increase in complexity. For this reason, conservative processing delays of one second (1s) are included in the case studies presented in Section 5. For the interested reader, an in-depth look at the theory behind the PF, and its mathematical formulation are provided in [19]. Furthermore, multiple variations of Bayesian filters, including the PF are compared in [20].

3.2. Synchrophasors

Synchrophasors are electrical measurements sharing a common reference. These measurements are commonly synchronized via GPS clocks. Figure 2 offers a basic depiction of the framework.

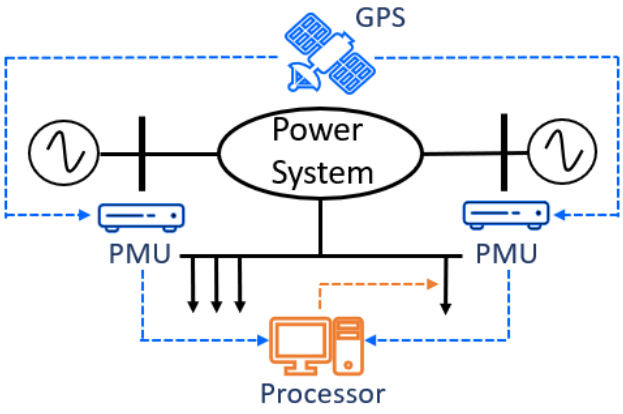

Figure 2. Overview of the architecture.

Devices that support synchrophasors are referred to as phasor measurement units or PMUs. PMUs have relatively high sampling rates, in some cases up to 120 frames per second (fps) [21]. These sampling rates combined with the synchronization of measurements, make it possible to derive input-output pairs that can be used to build mathematical models [22].

One common assumption made by PMU-based solutions is that high PMU sampling rates will be viable. Sampling rate limitations are in part driven by the capacity of communi-

Preprints (www.preprints.org) | NOT PEER-REVIEWED | Posted: 20 April 2023 doi:10.20944/preprints202304.0599.v1

cation networks. High PMU sampling rates could overwhelm communication networks in terms of data transfer and data storage [11,22]. With these limitations in mind, 30 fps seems to offer a balance between practicality, and estimation accuracy. Estimation across multiple sampling rates are performed in [23], with 30 fps delivering an acceptable performance relative to higher sampling rates. Moreover, high frequency signals are not typically studied in frequency stability applications.

3.3. Disturbance Detection

Techniques that utilize derivatives or rate of change, to detect frequency disturbances are referred to as *semi-adaptive* techniques [24]. Semi-adaptive techniques offer a good balance between security and dependability [25]. In this work, the frequency rate of change R, is used as the primary means of disturbance detection. R can be computed as:

$$R = \frac{f_2 - f_1}{dt} \tag{11}$$

In equation 11, f_1 refers to the frequency at the start of the measurement period, and f_2 is frequency at the end of the period. dt represents the duration of period in seconds. One of the benefits of semi-adaptive detection is that it allows for intentional delays to be part of the scheme. These delays give the system a brief opportunity to self-correct issues before further action is taken. The duration of these delays is inversely proportional to R. In this work, the thresholds and their respective delays were taken from [26], and they are as follows:

Table 1. Frequency Rate of Change and corresponding delays.

Frequency Rate of Change (Hz/sec)	Time Window (Cycles)
15.00-2.33	3
2.32-1.17	6
1.16-0.78	9
0.77-0.58	12
0.57-0.47	15
0.46-0.38	18
0.37-0.33	21
0.32-0.29	24
0.28-0.26	27
<0.25	30

3.4. Prediction

This work introduces a simple, yet effective way to predict the future state of frequency using the particle filter. By default the PF will make predictions, however, these predictions extend only $k+1$ time steps into the future [19]. The time horizon of these predictions can be extended without significant modifications to the PF algorithm if measurements are augmented with artificial data points. The idea here is to use measurements to derive artificial data points, which are then processed by the PF. The output of the PF are estimates based on historical data, the underlying system model, and artificial data. From the perspective of the user, since these estimates are in the future, they can be considered a prediction. The artificial data points (ADPs) are computed as follows:

$$ADP_i = ADP_{i-1} + t_s f' + t_s^2 f'' \tag{12}$$

Where ADP_{i-1}, is the previous ADP, or the last measurement when $i = 1$. f' and f'' are the first and second frequency derivatives respectively. t_s represents the time window of the derivatives. These derivatives play a key role in determining the degree of influence system dynamics have on the ADPs. Derivatives calculated using only a few measurements leads to a set of ADPs that is very dynamic (sensitive to changes), which can be useful in some situations, this is explored in the case studies. The number of measurements used

Preprints (www.preprints.org) | NOT PEER-REVIEWED | Posted: 20 April 2023 doi:10.20944/preprints202304.0599.v1

in the derivation of the ADPs can be adjusted to increase (or decrease) the sensitivity of the algorithm to system dynamics as desired. This is similar to the tuning of Q and R parameters in the KF. These parameters are tuned to find a balance between new and historical data [15]. A compromise was found by averaging the change of the last ten measurements and then dividing this value by t_s. One can think of this as an average derivative. ADP computation is a sequential process that starts with the last measurement received. The derivatives are then used to adjust the previous ADP to produce the next one. The result is a vector containing the ADPs that will be the basis of predictions.

The time horizon of the prediction can be adjusted based on the number of ADPs used. For a desired time horizon, t_p, the desired number of ADPs can be found per:

$$N_{ADP} = \frac{t_p}{f_s} \tag{13}$$

The number of ADPs, N_{ADP}, is a function of the sampling rate f_s, and the time horizon of the prediction, t_p, which is measured in seconds. The process of ADP generation is summarized as follows:

Algorithm 2 ADP Generation

Initialisation:
ADP_{i-1} = Last measurement
f' = Average first derivative in last 10 measurements
f'' = Average second derivative in last 10 measurements
N_{ADP} = Number of ADPs required
1: **for** $i = 1$ to N_{ADP} **do**
2: $ADP_i = ADP_{i-1} + t_s f'$
$f' = f' + t_s f''$
3: **end for**

In this work, after an initial prediction is made, subsequent predictions are made with an emphasis on new data. Before a follow-up load shedding stage is executed, synchronisation between the machines is considered. Surprisingly, synchronisation is often overlooked in frequency stability solutions in literature [22]. In this work, machine rotor angles are assumed to be tracked via relays at the same sampling rate used for frequency, and the difference between the rotor angles, $\Delta\theta$, together with the predicted state of frequency, are used to determine the need for follow-up load shedding stages. This aspect of the solution will explored in the case studies presented in Section 5.

3.5. Excess Loading Equations

After a prediction indicating the need for corrective action is made, predicted frequency values are used to calculate the corresponding load excess L. Load excess can be calculated via the following expression, which is itself derived from the swing equation [27]:

$$L = \frac{RH(1 - \frac{f_2^2}{f_1^2})}{p(f_2 - f1)} \tag{14}$$

Here parameter f refers to frequency measurements. f_1 is the frequency at the beginning, while f_2 is the frequency at the end of the measurement period. R is the frequency rate of change, found via equation equation 11 . p is the power factor, and the inertia coefficient is represented by H. When L is calculated using predicted values, a modified version of equation 14 is used to calculate the corresponding predicted load excess L_p:

$$L_p = \frac{R_p H_{est}(1 - \frac{f_p^2}{f_1^2})}{p(f_p - f_1)} \tag{15}$$

 doi:10.20944/preprints202304.0599.v1

In equation 15, f_p is the predicted frequency. R_p is still the frequency rate of change, but now this parameter is calculated as the change from f_1, to the predicted frequency f_p, over the prediction period. Power factor p is calculated the same before, meanwhile H_{est}, is now an estimated coefficient of inertia. The process of obtaining H_{est} is described in the next section.

3.6. Online H Estimation

A common challenge encountered by power system stability solutions is the lack of reliable inertia (H) information [28]. Historically, these calculations have taken place during outages, by injecting test signals into the system and then analysing the response [29]. This approach proved to be reliable for decades, but now as the complexity of the grid continues to increase, inertia is evolving into a more dynamic parameter. Loads and renewable sources such as wind and solar, all have temporal characteristics that impact the inertia of the system [30,31]. Other events such tie lines closing can also lead to drastic changes in inertia [29].

With these challenges in mind, it becomes evident that a new approach to inertia estimation is needed. The sampling rates and synchronisation of PMUs make it possible to utilize system identification algorithms to estimate power system parameters [22]. One such approach, subspace estimation, has delivered encouraging results in power systems applications [23,32,33]. This work adopts an H estimation approach presented in [34], where H is estimated online from frequency and power measurements. As presented in [34], the online H estimation algorithm is not compatible with the framework developed in this paper. The original formulation utilizes high PMU sampling rates (100 fps), and the necessary data is collected over long time windows. Therefore, two simple modifications are made:

1. The sampling rate is decreased to 30 fps, a much more manageable data transfer rate [11,35].
2. Estimation of H is carried out periodically as opposed to in real-time. Historical data and forecasts can be used to reduce the number of times H is estimated. This work uses dynamic loading (modeled from real life data available at [36]), and the procedure is run the equivalent of six times per day. In the case studies presented in Section 5, H is assumed to have been estimated roughly two hours before the events take place.

3.7. Optimizing the Response

Mixed Integer Linear Programming (MILP) is used to optimize the corrective actions of the method. An objective function is minimized subject to a set of constraints. The algorithm then iterates and finds an optimal solution.

In terms of cost, in this work, DERs are given the lowest penalty among the three sources of compensation. This is followed by non-critical loads (i.e., residential loads). Sensitive loads carry the highest cost as these represent industrial operations where an outage can lead to significant losses in revenue or equipment damage. Critical or life-safety loads were not considered in this work as these are usually not intentionally dropped [27].

Preprints (www.preprints.org) | NOT PEER-REVIEWED | Posted: 20 April 2023 doi:10.20944/preprints202304.0599.v1

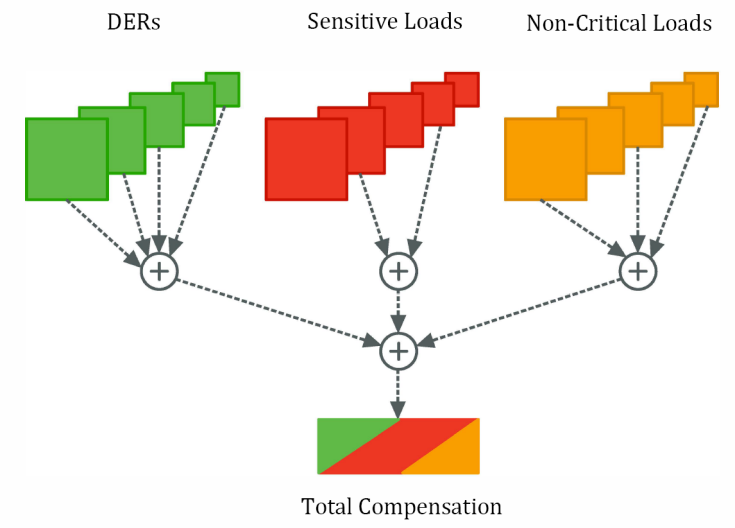

Figure 3. Compensation agent selection via optimization.

When deciding which agents to use, in addition to cost, the algorithm also considers factors such as distance from the disturbance, and the number of customers affected. For instance, it might be more desirable to drop one large industrial load instead of a large number of residential customers. Additional parameters can be added as required, and all parameters can be modified to meet a desired operational standard.

The information fed to the algorithm (capacity and loading information), is already collected at the substation level and transmitted to control centers [40]. This step would not place a significant burden on communication networks since all it requires is a periodical loading and capacity update. The task of optimizing load excess compensation can be summarised as follows:

Algorithm 3 Load Balance Optimization

Initialisation:
A = DER capacity available
B = Sensitive loads available to be shed (feeder level)
C = Non-critical loads available to be shed (feeder level)
c_1^T = Cost of DER actuation
c_2^T = Cost of shedding sensitive loads
c_3^T = Cost of shedding non-critical loads
b = Calculated load excess

1: **Minimize** J = $c_1^t x + c_2^t y + c_3^t z$
s.t. $Ax + By + Cz \geq b$
2: **Return** Selected agents in A, B, and C

As previously stated, the optimization routine can be easily modified to include additional agent types, costs, or constraints. After the optimal combination of DERs and loads for compensation have been identified, a trip signal is sent to the selected feeder breakers.

4. Distributed MPC Method Overview

This method is intended to operate as a distributed solution overseeing the frequency stability of an area of the grid. PMUs at the edge of an area share information with selected PMUs at neighboring areas, as depicted in Figure 4.

Preprints (www.preprints.org) | NOT PEER-REVIEWED | Posted: 20 April 2023 doi:10.20944/preprints202304.0599.v1

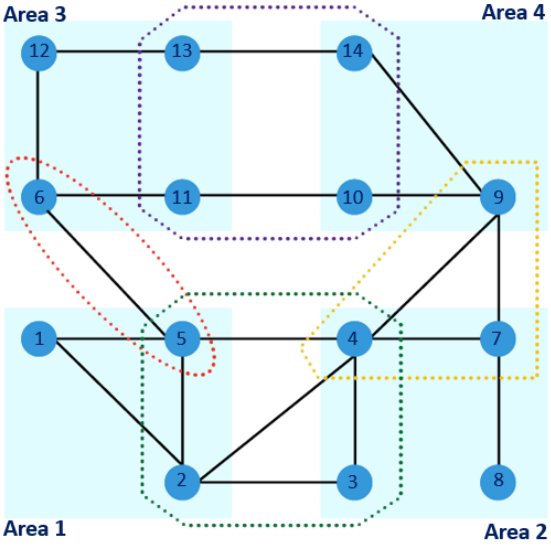

Figure 4. Overview of the architecture in distributed form.

When a disturbance is detected, the future state of frequency is predicted. Using the predicted value, a load excess is estimated. An optimization routine then evaluates the sources available for compensation such as DERs or load shedding, and identifies an optimal combination of agents to be actuated to regain generation-load balance. Figure 5 shows the modules that make up this proposed solution.

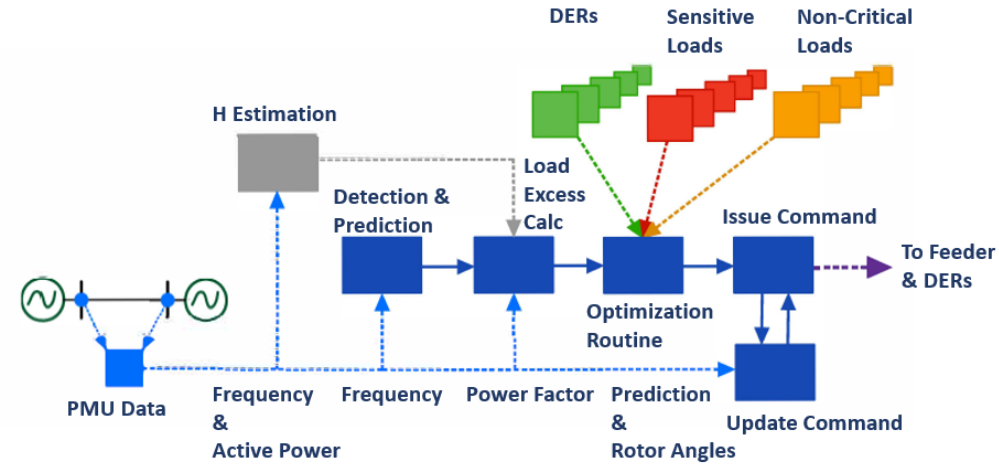

Figure 5. Overview of the algorithm and its modules.

Related techniques in literature assume a processing time of roughly 500 ms. In this context, computation time is assumed to be 400 ms (including communication delays), another 100 ms is added to account for relay processing time and breakers delays [5,6]. In this work a conservative delay of one full second is used.

Many of the operating parameters of this scheme are customizable, facilitating compliance with industry standards such as NERC PRC-006 [1]. Some of the ways this framework follows PRC-006 guidance include among others:

- Adjustable frequency thresholds.
- Adjustable number of load-shedding stages.
- Customizable islands (based on PMU availability).

Preprints (www.preprints.org) | NOT PEER-REVIEWED | Posted: 20 April 2023 doi:10.20944/preprints202304.0599.v1

- Additional parameters such as voltage levels, frequency overshoot, rotor angles, breaker status, and loading of power lines can be integrated as constraints as long as the networks can support it.
- This method eliminates the need for simulations to establish underfrequency load-shedding (UFLS) contingencies.

A data flow diagram of the method is presented in Figure 6.

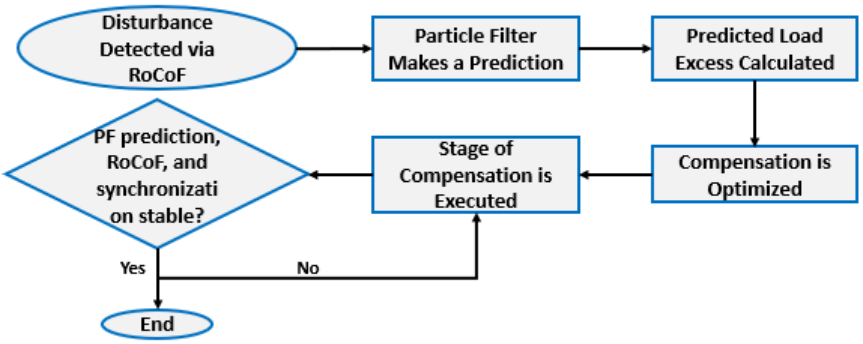

Figure 6. Data flow diagram of the method.

5. Case Studies

This section contains three case studies that showcase the advantages of the presented method under different operating conditions and constraints. Each case study includes key performance metrics as well as comparisons with other methods found in literature. Before proceeding to the test cases an illustrative example is presented. The purpose of the example is to summarize the topics and steps discussed in the previous sections.

5.1. Illustrative Example

Figure 7 illustrates the complete response of a four-machine system after a disturbance is introduced and mitigated using the scheme presented in this work.

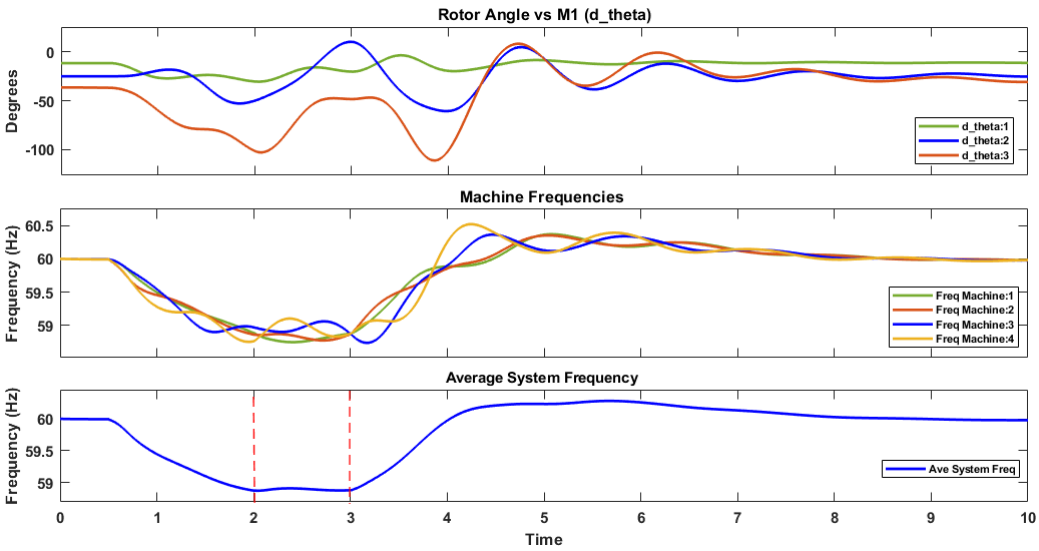

Figure 7. Multi-Stage compensation based on predictions.

The disturbance starts at 0.5s, and it is detected via the RoCoF from equation 11. At 1s, a prediction is made as shown in Figure 8.

Preprints (www.preprints.org) | NOT PEER-REVIEWED | Posted: 20 April 2023 doi:10.20944/preprints202304.0599.v1

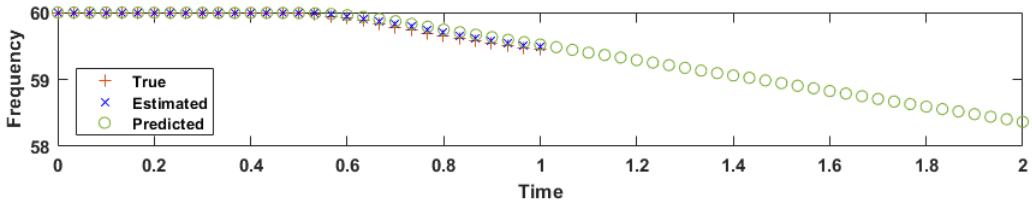

Figure 8. First particle filter prediction.

The method estimates the state of the system frequency one second into the future. These estimates are then used to calculate the loading excess via equation 15, which is then followed by a compensation stage at 2s, as seen in Figure 7. A second prediction is made immediately after the first stage of compensation, this is shown in Figure 9.

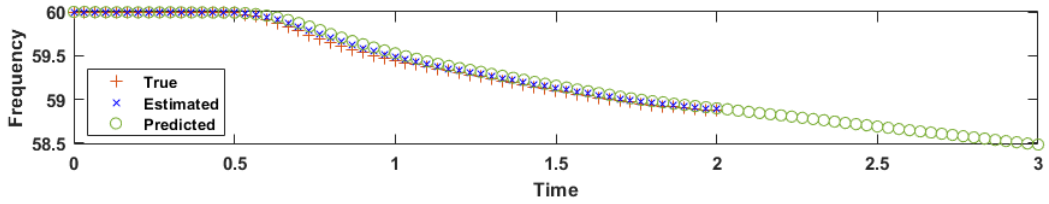

Figure 9. Second particle filter prediction.

Based on this new prediction, a second stage of compensation is executed at 3s, which then followed by a third prediction, illustrated in Figure 10.

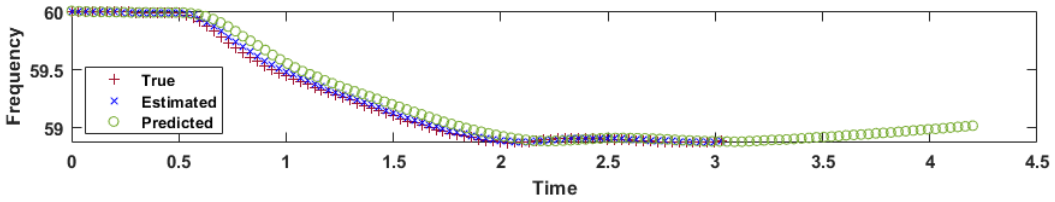

Figure 10. Third particle filter prediction.

The third prediction shows that the frequency is trending back into stability. Since frequency is expected to return to its normal range, a third stage of compensation is not executed. In this case the system regains stability with minimal overshoot as seen in Figure 11.

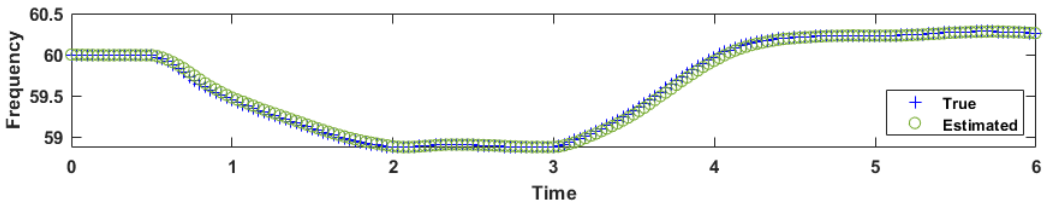

Figure 11. Complete response estimated by the particle filter.

Subsequent stages of compensation are not executed when three conditions are met:

1. The PF predicts a rise in frequency.
2. The RoCoF is positive.
3. Machine synchronization is stable. The goal of the method is to first stop the decay in frequency, and second, to send it back to a range where generator governors can stabilize it.

5.2. Case Study I

This case study contains four scenarios and it is based on Kundur's Two-Area System. This model can be found at [41]. The locations where excess loads are introduced to the

Preprints (www.preprints.org) | NOT PEER-REVIEWED | Posted: 20 April 2023 doi:10.20944/preprints202304.0599.v1

system are numbered (1 through 4) in Figure 12. Loading, capacity and other operational data are presented in Tables 2 and 3, and also in Table A1 in the ***Appendix*** section. To account for processing and communication delays, corrective actions are taken a full second after a prediction is made. Gaussian noise with a variance of 0.025 is added to the measurements.

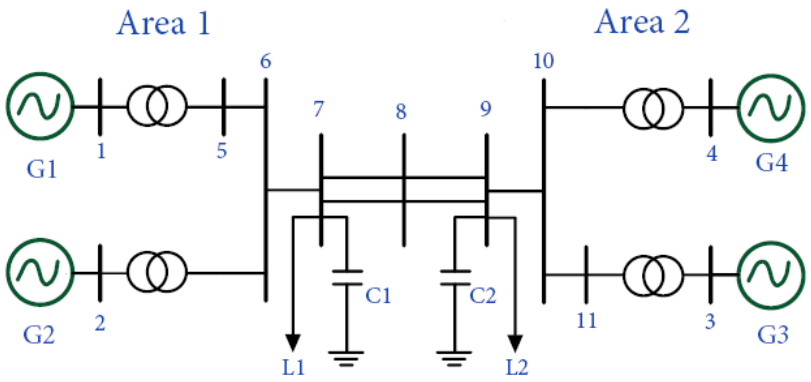

Figure 12. One line diagram of Case Study I.

Table 2. Load Flow Data

Bus	V	P_G	P_L	Q_L	Q_C
1	1.03	615	-	-	-
2	1.01	700	-	-	-
3	1.03	719	-	-	-
4	1.01	700	-	-	-
7	-	-	967	100	200
9	-	-	1767	100	350

Table 3. Generator Dynamic Data

Generator	Rating (MVA)	X_d	X'_d	X''_d	T'_{d0}	T''_{d0}	X'_q	X''_q	T'_{q0}	T''_{q0}	H
G1	900	1.8	0.3	0.25	8	0.03	1.7	0.25	0.4	0.05	6.5
G2	900	1.8	0.3	0.25	8	0.03	1.7	0.25	0.4	0.05	6.5
G3	900	1.8	0.3	0.25	8	0.03	1.7	0.25	0.4	0.05	6.175
G4	900	1.8	0.3	0.25	8	0.03	1.7	0.25	0.4	0.05	6.175

The scenario where the load excess is placed at bus 1 in Figure 12, is run twice. First, a fixed three stage compensation procedure is used. The first compensation stage is set at 50% of the calculated load excess. Stages 2 and 3 each compensate 25% of the load excess, for a total of 100%, similar to the approach used by [6]. For the second round, adjustable stages of compensation are used. The load imbalance starts at 0.5 seconds, and each compensation stage is marked by vertical dashed lines in Figure 13.

Preprints (www.preprints.org) | NOT PEER-REVIEWED | Posted: 20 April 2023 doi:10.20944/preprints202304.0599.v1

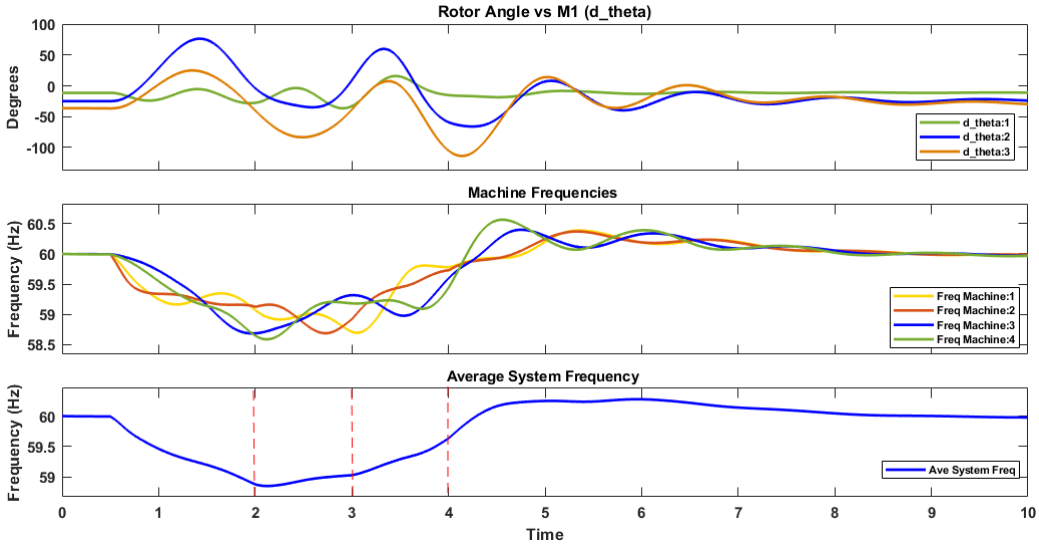

Figure 13. Case Study I, scenario 1 results.

In this case the system was successful in first, arresting the frequency decline, and second, in providing a smooth transition to steady state. Three predictions were made by the particle filter, they are shown below:

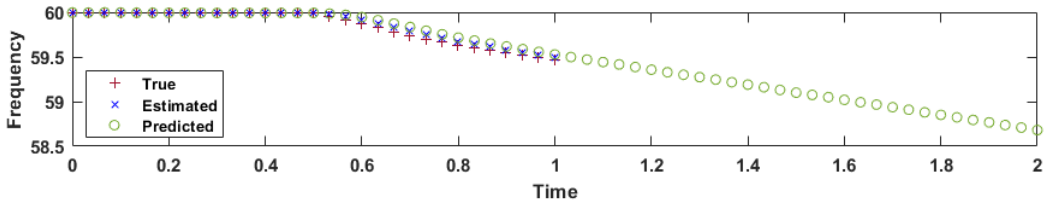

Figure 14. First prediction.

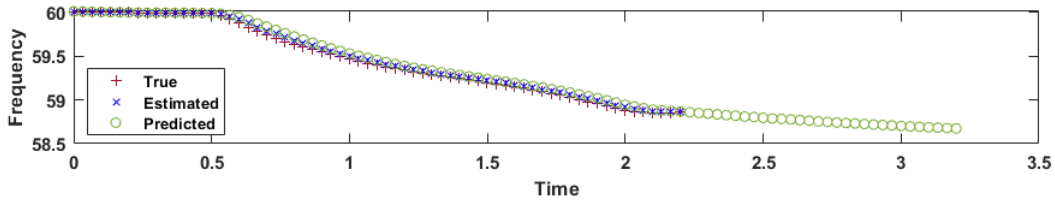

Figure 15. Second prediction.

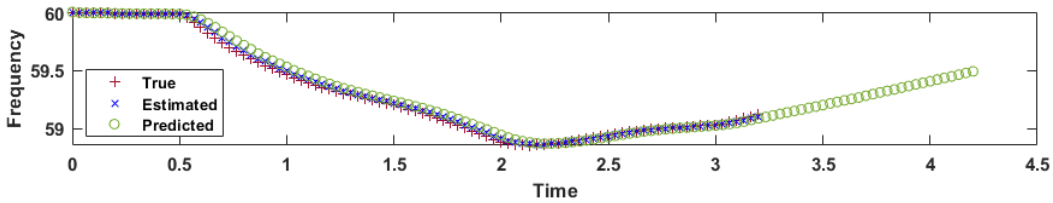

Figure 16. Third prediction.

This same scenario was performed using a version of the algorithm referred to as adaptive compensation. Adaptive compensation works as follows: The initial stage compensates for 50% of the estimated excess load factor. After the first stage is executed, the number of samples used in obtaining the derivatives in equation 12 is decreased, making the particle filter more receptive to system dynamics. Compensation with variable stages is illustrated in Figure 17.

Preprints (www.preprints.org) | NOT PEER-REVIEWED | Posted: 20 April 2023 doi:10.20944/preprints202304.0599.v1

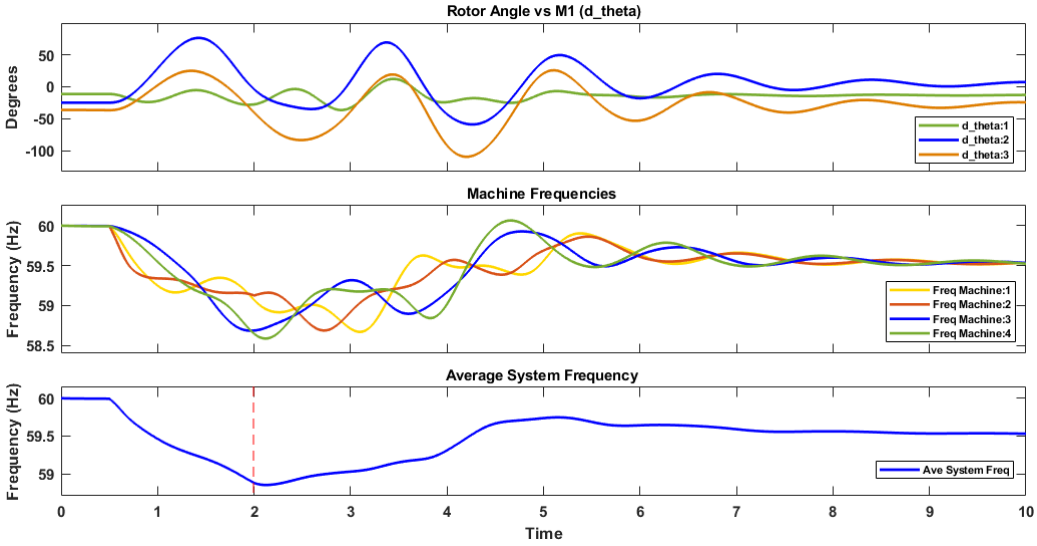

Figure 17. Scenario 1, PF compensation with adaptive stages.

In this case, the PF predicts that frequency will be returning to levels close to the reference after only one stage of compensation. This is shown in Figure 18.

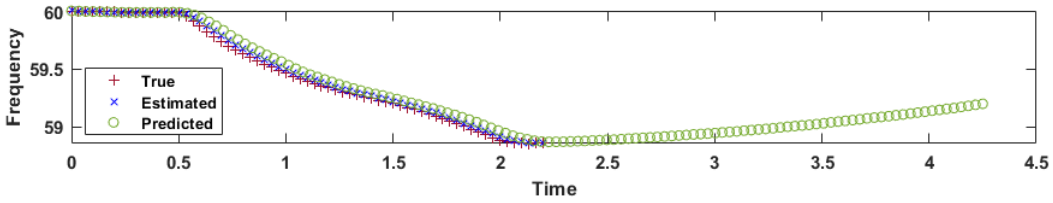

Figure 18. PF prediction after the first stage.

With frequency expected to return to its normal range, and $\Delta\theta$ not trending towards loss of synchronism, further compensation stages are avoided. Being able to restore frequency stability while compensating only a portion of the calculated load excess happens for two reasons: First, being able to take corrective actions early, means that compensation can begin before the system reaches a critical state. Second, generator governors and other controllers are not considered during compensation calculations, and while this might lead to some inaccuracies, it also gives the scheme a safety margin, which translates into a lower amount of load shed. Realistically, a highly accurate load compensation value is difficult to obtain given the time constraints and the dynamics of both the loads and the sources. Moreover, it has been suggested that in the context of stability, early action trumps accuracy [6].

This scenario is performed once again with the adaptive compensation procedure, but this time, polynomial curve fitting (PCF) as presented in [6], is used to obtain predictions instead of the PF. After the first stage of compensation has been executed, a follow up prediction is made as illustrated by Figure 19.

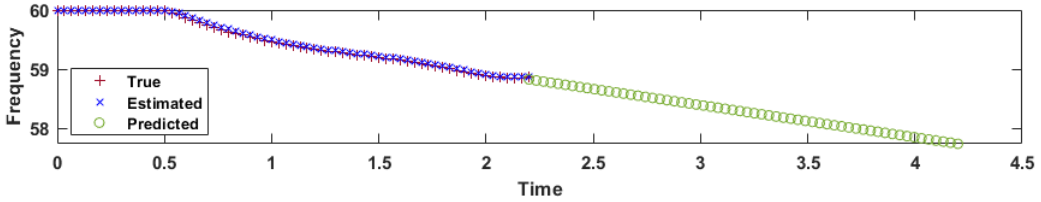

Figure 19. Prediction using PCF.

The prediction obtained via polynomial curve fitting is unable to leverage the dynamics of the system the way the PF can, leading to further stages of compensation.

Preprints (www.preprints.org) | NOT PEER-REVIEWED | Posted: 20 April 2023 doi:10.20944/preprints202304.0599.v1

Three more disturbances are introduced, and both the PF based method and the PCF technique are used to mitigate them. A performance comparison is presented in Table 4.

Table 4. Key Metrics for Case Study I.

Fault Location	Method	Number of Stages	% of Load Excess Compensated
1	PF	1	50%
	PCF	3	100%
2	PF	2	75%
	PCF	3	100%
3	PF	2	75%
	PCF	3	100%
4	PF	1	50%
	PCF	3	100%

For the four scenarios presented in Table 4, the method presented in this paper was able to bring the system back into stability while shedding 25% to 50% less load. This is, as previously discussed, due to the ability of the prediction model to leverage the dynamics of the system as frequency begins to revert back into stability.

Performance metrics are examined in Table 5, where frequency overshoot during recovery is measured.

Table 5. Overshoot values for Case Study I.

Fault Location	Number of Stages	Overshoot
1	1	-0.83%
2	2	1.13%
3	2	0.91 %
4	1	2.1%

As expected, more stages leads to a smoother transition back into steady state. It is worth noting that even when only one compensation stage was used, the overshoot was still fairly low.

5.3. Case Study II

A second case study was conducted in the IEEE 14 Bus System. Following the same process as the first case study, four scenarios are presented. The locations where the load excess is introduced during each scenario are presented in Figure 20. Loading, capacity and other operational data is presented in Table A2 in the ***Appendix*** section.

Preprints (www.preprints.org) | NOT PEER-REVIEWED | Posted: 20 April 2023 doi:10.20944/preprints202304.0599.v1

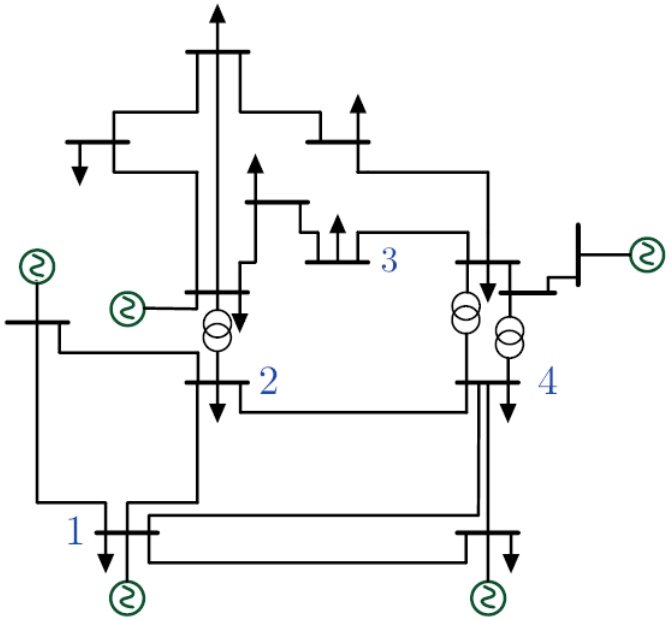

Figure 20. IEEE 14 Bus System used in Case Study II.

Once again, each scenario is ran twice, one time using PCF to build a base line and then using the PF. Key metrics are presented in Table 6.

Table 6. Key Metrics for Case Study II.

Fault Location	Method	Number of Stages	% of Load Excess Compensated
1	PF	1	50%
	PCF	3	100%
2	PF	2	75%
	PCF	3	100%
3	PF	1	50%
	PCF	3	100%
4	PF	1	50%
	PCF	3	100%

The results of this case study are consistent with the first one, and they show that the PF based method facilitates the recovery of frequency while greatly decreasing the amount of compensation used. Overshoot is also used as a performance metric for this case study, and the results are presented in Table 7.

Table 7. Overshoot values for Case Study II.

Fault Location	Number of Stages	Overshoot
1	1	2.3%
2	2	0.84%
3	1	-1.72 %
4	1	1.93%

The observed overshoot in this scenario is again fairly low, which is consistent with the results obtained in the first case study.

Preprints (www.preprints.org) | NOT PEER-REVIEWED | Posted: 20 April 2023 doi:10.20944/preprints202304.0599.v1

5.4. Case Study III

The goal of this final test case is to highlight the flexibility of the method and use it to drive Distributed Energy Resources (DERs) in real-time. This test was run under a similar set of assumptions as those made in [12], where a KF-based compensation method is presented. In order to test the algorithm under demanding conditions, faster frequency deviations than those seen in [12] were generated. Most importantly, the total delay time involved in the processing of data and actuation of DERs was increased to 500ms; up from the 40ms time delay used in [12]. That's a response time over ten times slower.

Frequency deviations start at 1s, with a significant loss in generation at 1.5s. As illustrated in Figure 21, DER actuation takes place 0.5s after the frequency deviations.

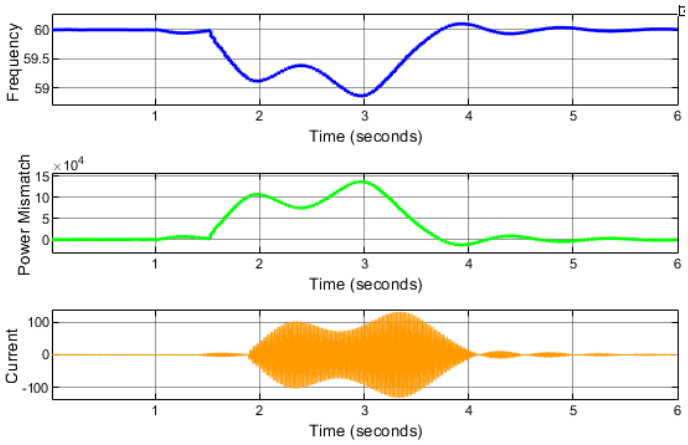

Figure 21. Real-Time mitigation via DERs.

As before, measurements are made via PMUs at 30 fps. The power mismatch is calculated continuously in this test case per equations 11 and 15 in the form of a controller. As shown in Figure 21 above, the frequency and power mismatch follow virtually the same trend but in opposite directions. When frequency deviates from the 60 Hz reference, a corresponding current output is seen from the DERs. The compensation is based on the power mismatch calculated by the controller. Despite a 0.5 second delay, the system successfully mitigates the frequency deviations.

6. Conclusions

This work presented a distributed MPC method for frequency stability of power systems. The method considers PMU observations and the particle filter. By being able to estimate the future state of frequency, corrective actions can be taken before the system reaches a critical condition. This proactive approach makes it possible to optimize the response to a disturbance thereby reducing the amount of compensation utilized. The method was tested via simulations based on Kundur's Two-Area System, and the IEEE 14-Bus system. The results were promising and outperformed other contemporary solutions by drastically reducing the mount of load dropped during compensation. As with essentially all PMU based solutions, limitations in communication networks drive the feasibility of the solution. Future work will focus on streamlining the solution by reducing requirements in terms of data and the number of PMUs utilized. Alternative optimization methods as well as improving the robustness of the particle filter will also be investigated.

Author Contributions: Conceptualization, G.P. and A.B.; methodology, G.P.; software, G.P.; validation, G.P.; formal analysis, G.P.; investigation, G.P.; resources, G.P.; data curation, G.P.; writing—original draft preparation, G.P.; writing—review and editing, G.P. and A.B.; visualization, G.P.; supervision, A.B.; project administration, G.P.; funding acquisition, A.B. All authors have read and agreed to the published version of the manuscript.

Funding: Not applicable

 doi:10.20944/preprints202304.0599.v1

Institutional Review Board Statement: Not applicable

Informed Consent Statement: Not applicable

Data Availability Statement: The data presented in this study are available on request from the corresponding author.

Conflicts of Interest: The authors declare no conflict of interest.

Abbreviations

DER	Distributed Energy Resource
KF	Kalman Filter
MILP	Mixed Integer Linear Programming
MPC	Model Predictive Control
PMU	Phasor Measurement Unit
PF	Particle Filter
RoCoF	Rate of Change of Frequency
UFLS	Underfrequency Load-Shedding

Appendix A

The tables below present the loading conditions for each case study. Total DER Capacity refers to the total additional power DERs can supply (rated power minus power supplied). This number is given as a percentage of the total rated power of the generators. Excess loading is also given as a percentage of the total rated power of the generators. Actual values for the first case study can be found at [41]. For the second case study, the IEEE 14 Bus System was used with default parameters. In both cases the loading was divided into groups so the algorithm described in Section 3.7 could be used.

Table A1. System loading and capacity for Case Study I.

Fault Location	Total DER Capacity	Excess Loading
1	5%	18%
2	3%	21%
3	6%	20%
4	8%	22%

Table A2. System loading and capacity for Case Study II.

Fault Location	Machine	Loading %	Total DER Capacity	Excess Loading
1	1 2 3 4 5	80% 85% 88% 90% 85%	5%	17%
2	1 2 3 4 5	80% 90% 85% 85% 80%	4%	21%
3	1 2 3 4 5	90% 88% 80% 80% 85%	5%	19%
4	1 2 3 4 5	85% 85% 85% 85% 85%	2%	20%

References

1. NERC Standards, PRC-006-SERC-02, 2017, Available online: https://www.nerc.com/pa/Stand/Pages/PRC006SERC02RI.aspx (accessed on 14 Feb. 2023).
2. IEEE. IEEE guide for the application of protective relays used for abnormal fre- quency load shedding and restoration. IEEE Std C37.117-2007; 2007. p. c1.
3. Rudez, U.; Mihalic R., "A novel approach to underfrequency load shedding, *Electric Power Systems Research*", **2011**, *81*, pp. 636-643, doi: 10.1016/j.epsr.2010.10.020.
4. Sigrist, L.; Egido, I.; Rouco, L., "Principles of a Centralized UFLS Scheme for Small Isolated Power Systems", *IEEE Transactions on Power Systemss*, **2013**, *28*, pp. 1779-1786, doi: 10.1109/TPWRS.2012.2227839.
5. Larsson, M.; Rehtanz, C., "Predictive frequency stability control based on wide-area phasor measurements", *IEEE Power Engineering Society Summer Meeting*, **2005**, *1*, pp. 233-238, doi: 10.3390/app112412148.
6. Rudez, U.; Mihalic R., "WAMS-Based Underfrequency Load Shedding With Short-Term Frequency Prediction", *IEEE Transactions on Power Delivery*, **2016**, *31*, pp. 1912-1920, doi: 10.1109/TPWRD.2015.2503734.
7. Bretas, A., Bretas, N., Massignan, J. & London Junior, J. Hybrid Physics-Based Adaptive Kalman Filter State Estimation Framework. *Energies*. **2021**, **14**, doi: 10.3390/en14206787.
8. Zhang, C., Zhao, S. & He, Y. "An Integrated Method of the Future Capacity and RUL Prediction for Lithium-Ion Battery Pack", *IEEE Transactions On Vehicular Technology*. **71**, 2601-2613, **2022**, doi: 10.1109/TVT.2021.3138959.
9. Zhao, S., Zhang, C. & Wang, Y. Lithium-ion battery capacity and remaining useful life prediction using board learning system and long short-term memory neural network. *Journal Of Energy Storage*. **52**, pp. 104901, **2022**, doi: 10.1016/j.est.2022.104901.
10. Zhang C, Zhao S, Yang Z & Chen Y, "A reliable data-driven state-of health estimation model for lithium-ion batteries in electric vehicles.", *Front. Energy Res.*, **2022**, doi: 10.3389/fenrg.2022.1013800.
11. Bose, A., "Smart Transmission Grid Applications and Their Supporting Infrastructure", *IEEE Transactions on Smart Grid*, **2010**, *1*, pp. 11-19, doi: 10.1109/TSG.2010.2044899.
12. Pulendran, S.; Tate, J.E., "Energy Storage System Control for Prevention of Transient Under-Frequency Load Shedding", *IEEE Transactions on Smart Grid* , **2017**, *8*, pp. 927-936, doi: 10.1109/TSG.2015.2476963.
13. Sauhats, A.; Utans, A.; Silinevics, J.; Junghans, G.; Guzs, D., "Enhancing Power System Frequency with a Novel Load Shedding Method Including Monitoring of Synchronous Condensers' Power Injections", *Energies*, **2021**, *14*, pp. 1490, doi: 10.3390/en14051490
14. Farantatos, E.; Huang, R.; Cokkinides, G.J.; Meliopoulos, A.P. A Predictive Generator Out-of-Step Protection and Transient Stability Monitoring Scheme Enabled by a Distributed Dynamic State Estimator. *IEEE Trans. Power Deliv.* **2016**, *31*, pp. 1826-1835, doi: 10.1109/TPWRD.2015.2512268.
15. Zhao, J.; et al., "Power System Dynamic State Estimation: Motivations, Definitions, Methodologies, and Future Work", *IEEE Transactions on Power Systems*, **2019**, *34*, pp. 3188-3198, doi: 10.1109/TPWRS.2019.2894769.

16. Wang, S.; et al., "Assessing Gaussian Assumption of PMU Measurement Error Using Field Data", *IEEE Transactions on Power Delivery*, **2018**, *33*, pp. 3233-3236, doi: 10.1109/TPWRD.2017.2762927.
17. Xu, Y.; Xu, K.; Wan, J.; Xiong, Z.; Li, Y., "Research on Particle Filter Tracking Method Based on Kalman Filter", *IEEE Advanced Information Management,Communicates,Electronic and Automation Control Conference (IMCEC)*, **2018**, pp. 1564-1568, doi: 10.1109/IMCEC.2018.8469578.
18. Li, T.; Sattar, T. P.; Sun, S., "Deterministic resampling: Unbiased sampling to avoid sample impoverishment in particle filters", *Signal Processing*, **2012**, *92*, pp. 1637-1645, doi: 10.1016/j.sigpro.2011.12.019.
19. Elfring, J.; et al., "Particle Filters: A Hands-On Tutorial", *Sensors*, **2021**, *21*, pp. 438, doi: 10.3390/s21020438.
20. Arulampalam, M. S.; Maskell, S,; Gordo, N.; Clapp, T., "A tutorial on particle filters for online nonlinear/non-Gaussian Bayesian tracking", *IEEE Transactions on Signal Processing* , **2002**, *139*, pp. 174-188, doi: 10.1109/78.978374.
21. "IEEE Standard for Synchrophasor Measurements for Power Systems", *IEEE Std C37.118.1-2011 (Revision of IEEE Std C37.118-2005)*, **2011**, pp.1-61, doi: 10.1109/IEEESTD.2011.6111219.
22. Paramo, G.; Bretas, A.; Meyn, S., "Research Trends and Applications of PMUs", *Energies*, **2022**, *15*, pp. 5329, doi: 10.3390/en15155329.
23. Paramo, G.; Bretas, A. S., "WAMS Based Eigenvalue Space Model for High Impedance Fault Detection", *Appl. Sci.* **2021**, *11*, 12148, doi: 10.3390/app112412148.
24. Anderson, P. M.; Mirheydar, M., "An adaptive method for setting underfrequency load shedding relays", *IEEE Transactions on Power Systems*, **1992**, *7*, pp. 647-655, doi: 10.1109/59.141770.
25. Rudez, U.; Mihalic, R., "Monitoring the First Frequency Derivative to Improve Adaptive Underfrequency Load-Shedding Schemes", *IEEE Transactions on Power Systems*, **2011**, *26*, pp. 839-846, doi: 10.1109/TPWRS.2010.2059715.
26. SEL-751 https://selinc.com/products/751 (accessed on 1 July 2022).
27. Horowitz, S. H.; Phadke, A. G., *Power System Relaying*, 4th ed.; Wiley: London, UK, 2014.
28. Sigrist, L.; Rouco, L.; Echavarren, F. M., "A review of the state of the art of UFLS schemes for isolated power systems", *International Journal of Electrical Power & Energy Systems*, **2018**, *99*, pp. 525-539, doi: 10.1016/j.ijepes.2018.01.052.
29. Kundur, P., *Power System Stability and Control*, 2nd ed.; McGraw-Hill: New York, NY, USA, 1994.
30. Knap, V.; et al., "Sizing of an Energy Storage System for Grid Inertial Response and Primary Frequency Reserve", *IEEE Transactions on Power Systems*, **2016**, *31*, pp. 3447-3456, doi: 10.1109/TPWRS.2015.2503565.
31. Keung, P. K.; Li, P.; Banakar, H.; Ooi, B. T., "Kinetic Energy of Wind-Turbine Generators for System Frequency Support", *IEEE Transactions on Power Systems*, **2009**, *24*, pp. 279-287, doi: 10.1109/TPWRS.2008.2004827.
32. Nezam Sarmadi, S. A.; Venkatasubramanian, V.; Thomas, R.J., "Electromechanical Mode Estimation Using Recursive Adaptive Stochastic Subspace Identification", *IEEE Transactions on Power Systems*, **2014**, *29*, pp. 349-358, doi: 10.1109/TPWRS.2013.2281004.
33. Kim, J.; Tong, L.; Thomas, R.J., "Subspace Methods for Data Attack on State Estimation: A Data Driven Approach", *IEEE Transactions on Signal Processing* **2015**, *63*, pp. 1102-1114, doi: 10.1109/TSP.2014.2385670.
34. Zeng, F., et al., "Online Estimation of Power System Inertia Constant Under Normal Operating Conditions", *IEEE Access*, **2020**, *8*, pp. 101426-101436, doi: 10.1109/ACCESS.2020.2997728.
35. Naduvathuparambil, B.; Valenti, M. C.; Feliachi, A., "Communication delays in wide area measurement systems", *Proceedings of the Thirty-Fourth Southeastern Symposium on System Theory (Cat. No.02EX540)*, **2002**, pp. 118-122, doi: 10.1109/SSST.2002.1027017.
36. ERCOT Grid Info: Load, Loading Data, 2022, Available online: http://www.ercot.com/gridinfo/load (accessed on 8 Oct. 2022).
37. Parisio, A.; Rikos, E.; Glielmo, L., "A Model Predictive Control Approach to Microgrid Operation Optimization", *IEEE Transactions on Control Systems Technology*, **2014**, *22*, pp. 1813-1827, doi: 10.1109/TCST.2013.2295737.
38. Floudas, C. A.; Lin, X, "Mixed Integer Linear Programming in Process Scheduling: Modeling, Algorithms, and Applications", *Annals of Operations Research* , **2005**, *139*, pp. 131–162, doi: 10.1109/61.568226.
39. Carrion, M.; Arroyo, J. M., "A computationally efficient mixed-integer linear formulation for the thermal unit commitment problem", *IEEE Transactions on Power Systems*, **2006**, *21*, pp. 1371-1378, doi: 10.1109/TPWRS.2006.876672.
40. Schweitzer, E. O.; Whitehead, D.; Zweigle, G.; Ravikumar K. G.; Rzepka, G., "Synchrophasor-based power system protection and control applications", *2010 Modern Electric Power Systems, Wroclaw, Poland*, 2010, pp. 1-10, doi: 10.1109/CPRE.2010.5469481.
41. Kundur, P., "Simplified Synchronous Machine - Speed Regulation", *MathWorks*, https://www.mathworks.com/help/sps/ug/pmu-pll-based-positive-sequence-kundur-s-two-area-system.html;jsessionid=9f7bc00182f35350d6b467d0cb3c (accessed on 1 Nov. 2022).